International Journal of Mass Spectrometry 276 (2008) 43–48

Contents lists available at ScienceDirect

International Journal of Mass Spectrometry

journal homepage: www.elsevier.com/locate/ijms

Dissociation of methanol by ion-impact: Breakup dynamics, bond rearrangement and kinetic energy release

Sankar De[a,b,*], A. Roy[a], Jyoti Rajput[a], P.N. Ghosh[b], C.P. Safvan[a]

[a] Inter-University Accelerator Centre, Aruna Asaf Ali Marg, New Delhi 110067, India
[b] Department of Physics, University of Calcutta, 92 Acharya Prafulla Chandra Road, Kolkata 700009, India

ARTICLE INFO

Article history:
Received 23 April 2008
Received in revised form 27 June 2008
Accepted 27 June 2008
Available online 9 July 2008

Keywords:
Molecular dissociation
Time-of-flight mass spectrometry
Coincidence technique
Intramolecular bond rearrangement
Kinetic energy release

ABSTRACT

The dissociation dynamics of multiply charged methanol molecules formed in collision with 1.2 MeV Ar^{8+} projectiles is studied. Using coincidence mapping techniques, we can separate out the different dissociation pathways between carbon, oxygen and hydrogen ionic fragments as well as two- and three-body breakup events. Reactions involving intramolecular bond rearrangements within the CH_3 group of the dissociative molecule are discussed in detail. A signature of hydrogen migration in doubly charged methanol is observed. Kinetic energy releases of different breakup channels are reported here and compared with values calculated from a Coulomb explosion model. The shape and orientation of the islands in the coincidence map give further information about the momentum balance in the fragmentation process of two- or many-body dissociation pathways.

1. Introduction

In contrast to small molecules (diatomic and triatomic) and clusters, the study of Coulomb explosions for polyatomic molecules is scarce and details of the explosion processes are not clearly understood. In ion-molecule collisions, an unstable parent molecular ion is formed. Thereafter, dissociative ionization proceeds through different channels providing different dissociation products, both fragment ions and neutral atoms or molecular species. Although neutral products can be detected using charged particle detectors, their mass is difficult to determine. Hence their contribution to dissociation processes lead to greater complexity in data analysis and a complete assignment of breakup partners is difficult. Recently, the extensive use of multihit coincidence methods employing a position sensitive time-of-flight (TOF) measurement system [1] has provided an useful tool to unravel the dynamics of the dissociation processes of polyatomic molecules on impact of highly charged ions (HCI).

We are interested in studying the dissociation dynamics of simple hydrocarbon molecules containing the methyl group, induced by highly charged ion (HCI) impact. In the present study, we have chosen methanol as the first step of our investigation. Quite early, Eland and Treves-Brown [2] had used photoelectron–photoion–photoion coincidence (PEPIPICO) methods to find out a large number of breakup pathways of doubly charged methanol produced by photoionization at vacuum ultraviolet wavelengths. Bond rearrangement had also been extensively studied by the method of charge separation mass spectrometry for a number of organic methyl compounds using the PEPIPICO technique [3]. In another study on the field ionization and Coulomb explosion of methanol in an intense field of a femtosecond laser, Ren et al. [4] used a time-of-flight (TOF) mass spectrometer to calculate the kinetic energy release (KER) from the Coulomb explosion of highly charged parent ion and discussed the possible channels based on a kinetic model. Recently, from the intensive studies on hydrocarbons in an intense laser field, it has been revealed that a variety of dynamical processes accompanying ultrafast hydrogen atom transfer are induced. Yamanouchi and co-workers [5,6] have systematically investigated the dissociative ionization processes of methanol and its deuterated isotopomers by the methods of mass-resolved momentum imaging (MRMI) and coincidence momentum imaging (CMI) in order to clarify how the competing processes of the hydrogen-atom migration and the ejection of hydrogen molecular ions are induced in intense laser fields prior to the skeletal C–O bond breaking.

In an earlier study [7], we have investigated the dynamics of the hydrogen atoms within the doubly charged methanol molecular ions due to intramolecular bond rearrangement characterized

* Corresponding author. Present address: J.R. Macdonald Laboratory, Physics Department, Kansas State University, Manhattan, KS 66506-2601, USA.
Tel.: +1 785 532 2666.
E-mail addresses: sankar@phys.ksu.edu (S. De), safvan@iuac.res.in (C.P. Safvan).

1387-3806/$ – see front matter © 2008 Elsevier B.V. All rights reserved.
doi:10.1016/j.ijms.2008.06.021

by the ejection of diatomic and triatomic hydrogen molecular ions induced by intense HCI-induced fields. In the present article, we report further results of dissociation of multiple charged CH_3OH molecules in collision with 1.2 MeV Ar^{8+} projectiles. From the coincidence spectra between the fragments, we have separated out the different dissociation channels and measured the kinetic energy release (KER) of nearly all breakup pathways. Also by studying the shape and orientation of the islands in the coincidence spectra, we gain information about the momentum balance in the fragmentation processes for two- and many-body events.

2. Experimental details

Details of the experimental apparatus and data acquisition methodology for molecular fragmentation studies has been described elsewhere [8]. Here we only give a brief account of the setup. The experiment has been carried out in the Low Energy Ion Beam Facility (LEIBF) of Inter-University Accelerator Centre (IUAC), India. In the experiment, 1.2 MeV Ar^{8+} projectiles produced from the electron cyclotron resonance (ECR) ion source were transported to the collision chamber where they interact with the alcohol molecules effusing from a needle at right angle to the ion beam. Methanol molecules reach the needle through a clean vacuum line degassed by means of several freeze-pump-thaw cycles. The all metal gas line with the fine control valve was kept warm to avoid condensation of the vapours. Typical operating pressures were maintained in the range of 7×10^{-7} Torr whereas the ultra high vacuum chamber was kept at a base pressure of 9×10^{-8} Torr. The dissociated fragments were extracted from the interaction region into a linear, two-field time-of-flight mass spectrometer (TOFMS) by applying a uniform electric field perpendicular to both the ion beam and molecular gas-jet. At the exit of TOFMS, the dissociation products were detected by a position sensitive micro-channel plate (MCP) detector. Ejected electrons were extracted in the opposite direction of TOFMS and detected by a channel electron multiplier (CEM) detector which gives the trigger for starting the coincidence data acquisition. The stop signals from the MCP were recorded after proper amplification and discrimination from noise using standard nuclear electronics used for fast pulses. The TOF spectrum was acquired in multi-hit mode by a CAMAC-based time-to-digital converter (TDC) interfaced to a computer where several fragment ions were recorded in coincidence to obtain information on correlated dissociation products.

3. Results

3.1. Time-of-flight spectrum

The dissociation products observed from the TOF spectrum (Fig. 1) of methanol molecules show undissociated molecular ion like CH_3OH^+. The spectrum further shows fragments losing a hydrogen atom in steps due to the breakage of C–H and O–H bonds keeping the C–O part intact (CH_2OH^+, $CHOH^+$, COH^+, CO^+), to complete rupture of C–O skeleton producing charged atomic species like C^{q+} and O^{q+} where q varies from 1 to 3. One can also take a note of the relative intensities of the m/q peaks from 28 to 32 in the TOF spectrum. From the highest number of counts for CO^+, we can infer that a large number of multiply charged parent molecules looses all its C–H and O–H bonds rather than step by step bond cleavage. Probability of one proton loss from the CH_3 group is more than the loss of two, although the intensity is maximum when all the C–H bonds are broken. Another striking feature in the TOF spectrum is the detection of hydrogen molecular ions H_2^+ and H_3^+ at $m/q = 2$ and 3, whose origin will be described later. Charged atomic fragments originating from the Coulomb explosion of highly charged

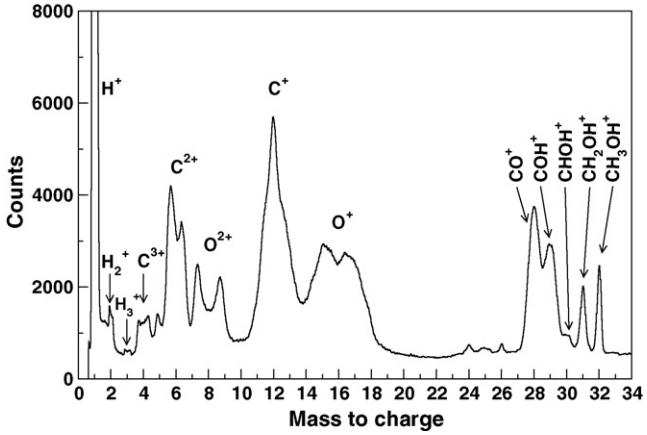

Fig. 1. Mass calibrated time-of-flight spectrum of dissociative CH_3OH.

parent molecular ions give rise to large KER. In the mass spectra, a broad peak of C^+ exhibits a large KER distribution. Similarly splitting into double peaks by other C^{q+} and O^{q+} ions demonstrate the expulsion of these ions with a relatively large kinetic energy in the forward and backward directions to the TOF extraction field. Interestingly enough, the C^+ peak is rather sharp in the TOF spectrum. This shows that a considerable population of the C^+ ions nearly stay at rest in the centre-of-mass system with KER close to 0 eV, whereas the protons and the O–H block emerge with a comparatively large momentum.

3.2. Coincidence map

To closely investigate the branching ratios of the different fragmentation channels and identify the two- and many-body dissociation pathways, we have generated coincidence maps (Figs. 2, 3 and 6) from the offline analysis of the acquired multi-hit data. This map is a two-dimensional spectrum between the TOF of the first fragment ion versus that of the second. It is a useful technique for the identification and separation of multi-particle events representing inter-particle correlations and have been used earlier

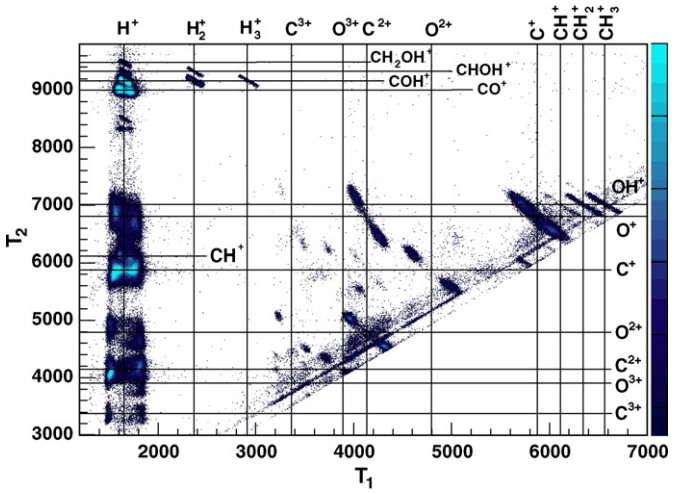

Fig. 2. Coincidence map showing dissociation channels between C^{q+} ($q = 1$–3) and O^{p+} ($p = 1$–3), H^+ and C^{q+} ($q = 1$–3) and H^+ and O^{p+} ($p = 1$–3) fragments. Events like $CH_3OH^{2+} \rightarrow CH^+_{(3-n)} + OH^+$ ($n = 0$–2) and breakup channels like $H^+ + CH^+$ are also observed. T_1 and T_2 are the time of flights of the first and second fragments. (For interpretation of the references to colour in this figure legend, the reader is referred to the web version of the article.)

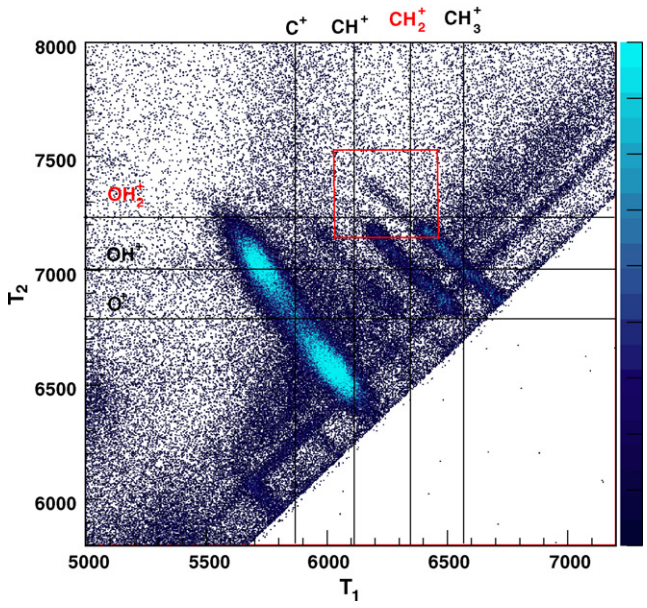

Fig. 3. Coincidence map showing hydrogen migration channel $CH_3OH^{2+} \rightarrow CH_2^+ + OH_2^+$ (within the box). (For interpretation of the references to colour in this figure legend, the reader is referred to the web version of the article.)

to study intramolecular bond rearrangements in doubly charged methanol [7].

From the two-dimensional coincidence map (Fig. 2), we had separated out the different dissociation channels corresponding to $C^{q+}(q = 1–3)$ and O^{p+} $(p = 1–3)$ fragments produced from complete rapture of C–O skeleton. Even two-body, three-body and four-body dissociation events such as:

$$CH_3OH^{2+} \rightarrow CH_3^+ + OH^+ \quad (1)$$

$$CH_3OH^{2+} \rightarrow CH_2^+ + OH^+ + \mathbf{H} \quad (2)$$

$$CH_3OH^{2+} \rightarrow CH^+ + OH^+ + \mathbf{2H} \quad (3)$$

respectively are observed where the C–O bond is broken keeping the OH part intact with the loss of hydrogen at every step. For more than two-body events the missing fragments (i.e., the ones that are in **boldface** in the equations) are either undetected neutrals or H^+ ions detected as a third or fourth hit in the MCP.

We observe the H^+ formation pathways in coincidence with C^{q+} $(q = 1–3)$ and O^{p+} $(p = 1–3)$ fragments in Fig. 2. The island corresponding to the $H^+ - C^+$coincidence, lies nearly horizontal to the C^+m/q line. This shows that the fragmented hydrogen ion takes away most of the energy leaving the singly charged carbon nearly at rest. This is not the case for $H^+ - O^+$ coincidence. Although of poor resolution, we can still note the detection of $H^+ + CH^+$ channel. On careful observation of the $H^+ - C^{2+}$ coincidence island, we found that it consists of two separate wings on either side of the C^{2+} line instead of just one as in the case of $H^+ - O^{2+}$ coincidence. We can think of two different processes as probable cause behind the occurrence of such opposite wings. The wing with higher intensity might be formed when both fragments (H^+ and C^{2+}) move in the same direction of the TOF extraction field after breakup of the CH_3 group. The other wing is possibly formed due to coincidence between C^{2+} of the methyl group and H^+ from O–H bond breakage traveling opposite to each other in the TOF extraction field just after dissociation. Such phenomenon has recently been observed in the case of H^+ and C^{q+} $(q = 1–3)$ coincidence, as reported by De et al. [9] in their ion-induced study of dissociative C_2H_2.

Concentrating on a specific area of the coincidence map (Fig. 2), we observed different fragmentation pathways leading to the breakage of one or many of the C–H bonds or the O–H bond in the multiply ionized methanol resulting in the formation of H^+, H_2^+ and H_3^+. We observed three two-body Coulomb explosion processes that form hydrogen atomic and molecular ions from doubly charged methanol:

$$CH_3OH^{2+} \rightarrow H^+ + CH_2OH^+ \quad (4)$$

$$CH_3OH^{2+} \rightarrow H_2^+ + CHOH^+ \quad (5)$$

$$CH_3OH^{2+} \rightarrow H_3^+ + COH^+ \quad (6)$$

Eq. (6) shows that H_3^+ is ejected from CH_3OH^{2+} due to two-body fragmentation process after intramolecular bond rearrangement has taken place within the methyl group of the molecule. But H_2^+ is formed due to both two-body (Eq. (5)) and three-body

$$CH_3OH^{2+} \rightarrow H_2^+ + COH^+ + \mathbf{H} \quad (7)$$

dissociation pathways also through rearrangement reactions. It should be noted that as soon as CO^+ is formed due to the disruption of the O–H bond, neither H_2^+ nor H_3^+ is recorded. It seems that the formation of H_2^+ and H_3^+ is a delicate phenomenon which gets disturbed as soon as the COH part is broken. These results along with a detailed study on the formation mechanism of H_3^+ have been published elsewhere [7]. Other than the above mentioned two-body channel (Eq. (4)), H^+ formation pathways are also through many-body processes:

$$CH_3OH^{2+} \rightarrow H^+ + CHOH^+ + \mathbf{H} \quad (8)$$

$$CH_3OH^{2+} \rightarrow H^+ + COH^+ + \mathbf{2H} \quad (9)$$

$$CH_3OH^{2+} \rightarrow H^+ + CO^+ + \mathbf{3H} \quad (10)$$

3.3. Hydrogen migration

Coulomb explosion dynamics competing with the hydrogen atom transfer from the methyl group to the nitrile group (CN) in CH_3CN [10] or to the hydroxyl group in CH_3OH [5] had been investigated previously using ultrafast intense laser fields. A signature of hydrogen migration has been observed in doubly charged methanol due to ion-impact. The coincidence map in Fig. 3 shows the hydrogen migration channel

$$CH_3OH^{2+} \rightarrow CH_2^+ + OH_2^+ \quad (11)$$

where one of the H atoms migrates from the methyl group to the hydroxyl group (OH) prior to C–O bond breaking.

4. Discussions

4.1. Kinetic energy release (KER) of dissociation products

Using the coincidence data from Fig. 2, we have determined the KER of different dissociation channels. We deduced the KER (U_{ker}) of the dissociation process in the centre of mass frame using the following equation derived from simple kinematics for a linear TOFMS [7]

$$\Delta T_s = \frac{2(2mU_{ker})^{1/2}}{qE} \quad (12)$$

where ΔT_s is the time separation between forward and backward emitted fragment peaks, q is the ionic charge, E the extraction field used in our TOFMS and m is the mass of the ion.

Fig. 4 shows the KER distributions of (a) H_2^+, (b) C^+ and (c) O^+ from different dissociation channels. A Gaussian is fitted to each

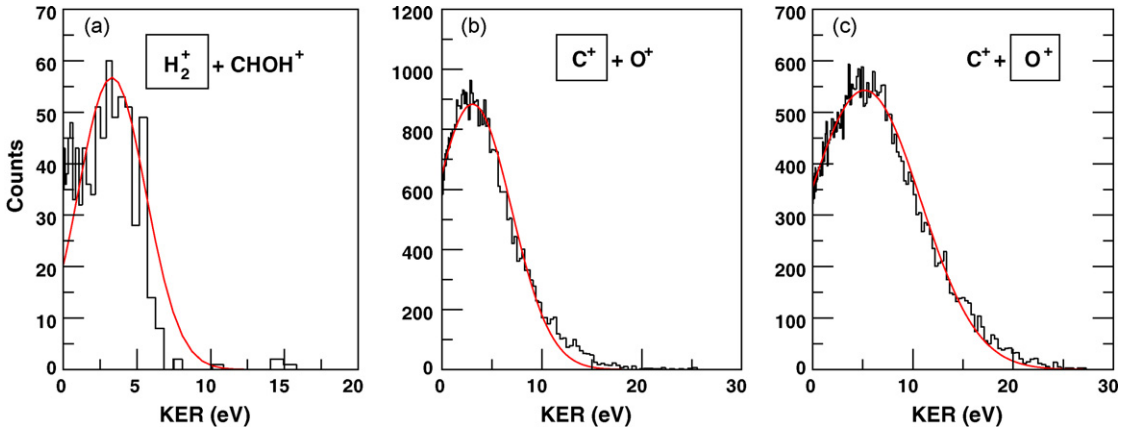

Fig. 4. Gaussian fit to the KER distributions of (a) H_2^+ (b) C^+ and (c) O^+. The corresponding dissociation channels are also shown. (For interpretation of the references to colour in this figure legend, the reader is referred to the web version of the article.)

of the distributions to find out the most probable KER values along with its width. The KER values of nearly all the dissociation channels designated in Fig. 2 are determined in the same way as above.

Table 1 lists the most probable (E_{prob}) and maximum (E_{max}) kinetic energies (in eV) producing H^+, H_2^+ and H_3^+ from CH_3OH due to 1.2 MeV Ar^{8+} impact. We have also compared our results with that obtained from photodissociation experiments [3]. The most probable values of KER for all the above ion-impact channels are lower than but comparable to the PEPIPICO values [3]. Table 1 shows that E_{prob} value of H^+ formation for channel number 5 has lower KER than that for channels 4 and 6. This trend is also observed in the case of photon studies. Increase in the KER value for channel 7 confirms a large amount of energy gained by the H^+ fragments due to all C–H and O–H bond cleavages. Four and five-body dissociation channels 6 and 7, respectively have a wider distribution in KER with respect to the two- and three-body channels 1–5. E_{prob} values for H_3^+ and H_2^+ formation from two-body breakup channels 1 and 2 are nearly the same. Possibly H_2^+ follows a similar minimum energy pathway during its formation as discussed for H_3^+ in Ref. [7].

Table 2 lists the most probable (E_{prob}) and total (E_{Total}) kinetic energies (in eV) for different dissociation channels producing C^{q+} + $O^{q'+}$ due to 1.2 MeV Ar^{8+} impact where the carbon and oxygen ionic charge states varies from 1 to 3 at different cases. We defined E_{Total} as the sum of most probable KER values of two dissociative species detected in coincidence. We also compared these results with that obtained from pure Coulomb explosion model (CEM). The value of KER is predicted by CEM (E_{Coul}) according to the relation:

$$E(\text{eV}) = 14.4\,\frac{q_1 \times q_2}{R(\text{Å})} \qquad (13)$$

where q_1 and q_2 are the charges on the two fragment ions and R (Å) is the internuclear distance of the neutral parent molecule. We have calculated the theoretical values of Coulombic KER taking the C–O bond length of the equilibrium geometry of neutral CH_3OH, $R_{C-O} = 1.37$ Å[4]. On comparing the total energy values with the theoretical KER values calculated from pure CEM, we observe a fairly good agreement between the two except a few cases. Therefore we can say that the highly charged CO moiety 'Coulomb' explodes as evident from the matching KER values between the experiment and CEM. Table 2 also lists the E_{prob} and E_{Total} values for two-body ($CH_3^+ + OH^+$) and detected twins from three-body ($CH_2^+ + OH^+ + \mathbf{H}$) breakup channels. We observe nearly the same values of E_{Total} for both of them, quite similar to what was reported in the case of photoionization studies [3].

Fig. 5 shows the KER values for H^+ along with their Gaussian fits for dissociation channels producing $H^+ + C^{q+}$ ($q = 1$–3) and $H^+ + O^{q+}$ ($q = 1$–2) due to methanol breakup. These values are listed in Table 3. E_{prob} and E_{max} values for $H^+ + H^+$ breakup pathway are also listed. E_{max} is defined as the KER value corresponding to 10% of the maximum counts for a particular ion species from a breakup channel. In Table 3(except for $H^+ + H^+$ channel), the E_{prob} and E_{max} values correspond to the peak and 10% of the peak of the Gaussian distribution for each dissociation channel. For $H^+ + C^{q+}$ and $H^+ + O^{q+}$ channels, we observe a gradual increase in the E_{prob} values for the H^+ fragments with the increase in carbon and oxygen charge states. E_{max} values also increase with the increase in charge

Table 1
Most probable and maximum kinetic energies for different dissociation channels producing H^+, H_2^+ and H_3^+ from dissociative CH_3OH

No.	Dissociation products	Ion	KER (eV)		
			E_{prob}	E_{max}	E_{photon}
1	$H_3^+ + COH^+$	H_3^+	3.2	6.0	3.6
2	$H_2^+ + CHOH^+$	H_2^+	3.3	6.8	3.4
3	$H_2^+ + COH^+ + \mathbf{H}$	H_2^+	2.9	7.4	3.7
4	$H^+ + CH_2OH^+$	H^+	2.6	9.3	4.4
5	$H^+ + CHOH^+ + \mathbf{H}$	H^+	2.0	8.3	3.3
6	$H^+ + COH^+ + \mathbf{2H}$	H^+	3.2	17.5	4.5
7	$H^+ + CO^+ + \mathbf{3H}$	H^+	6.7	20.2	

Also listed are the values obtained from PEPIPICO experiments [3].

Table 2
KER values obtained for the fragmentation channels $C^{q+} + O^{q'+}$ ($q, q' = 1$–3)

Dissociation products	Ion	KER (eV)		
		E_{prob}	E_{Total}	E_{Coul}
$C^+ + O^+$	C^+	3.1	8.5	10.5
	O^+	5.4		
$C^{2+} + O^+$	C^{2+}	9.8	24.1	21.0
	O^+	14.3		
$C^+ + O^{2+}$	C^+	11.7	31.4	21.0
	O^{2+}	19.7		
$C^+ + O^{3+}$	C^+	19.5	43.1	31.5
	O^{3+}	23.6		
$C^{2+} + O^{2+}$	C^{2+}	19.6	42.9	42.0
	O^{2+}	23.3		
$C^{3+} + O^{2+}$	C^{3+}	26.4	61.8	63.0
	O^{2+}	35.4		
$CH_3^+ + OH^+$	CH_3^+	1.2	3.2	
	OH^+	2.0		
$CH_2^+ + OH^+$	CH_2^+	1.7	3.0	
	OH^+	1.3		

These values are compared with that from pure Coulomb explosion model. Also listed are the KER values for channels $CH_3OH^{2+} \rightarrow CH_{(3-n)}^+ + OH^+$ ($n = 0$–1).

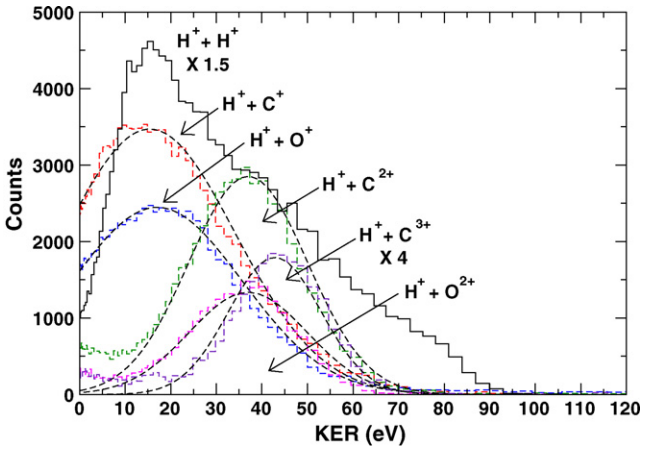

Fig. 5. KER distributions of H^+ fragments for $H^+ + H^+$, $H^+ + C^{q+}$ ($q = 1$–3) and $H^+ + O^{q+}$ ($q = 1$–2) dissociation channels. Each distribution except $H^+ + H^+$ is fitted with a Gaussian. (For interpretation of the references to colour in this figure legend, the reader is referred to the web version of the article.)

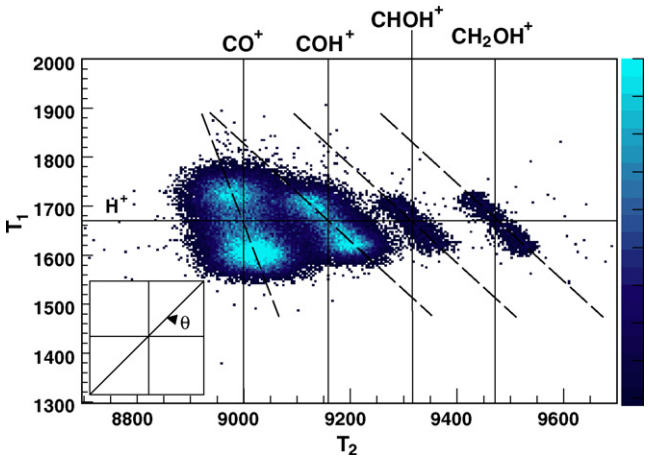

Fig. 6. Slopes drawn along the coincidence islands of $H^+ + CH_{(3-m)}OH^+$ ($m = 1$–3) and $H^+ + CO^+$ dissociation channels. Inset shows the angle θ of the slope.

states. It is observed that E_{prob} values for H^+ ions are nearly the same when the associate fragments have the same charge state (C^+, O^+ and C^{2+}, O^{2+}) irrespective of their mass. From Fig. 5, it is evident that the KER distribution for H^+ ions for $H^+ + H^+$ channel is mostly a convolution of KER spectra from all dissociation channels producing H^+ fragments due to H^+, C^{q+} ($q = 1$–3) and O^{q+} ($q = 1, 2$) coincidence breakups. All the above channels have contributions from both CH_3 and OH bond cleavages.

4.2. Slope of islands in the coincidence map

The geometrical properties of an island in the coincidence map, i.e., the shape, size and orientation, contain useful information for studying the dissociation dynamics. These include the KER distribution, ejection direction of the dissociated fragments and the dissociation sequence. An analysis of the covariance mapping in the mass spectrum has shown that the structure of the island is a momentum contour [11,12] where the length of the island reflects the kinetic energy of the ion pair and the slope gives information about the charge and momentum of the involved particles. If one or more fragments are not detected, the structure is broadened due to the momentum carried away by the undetected fragments.

The ion time-of-flight T is a linear function of the projection of the ion's initial momentum **P** along the spectrometer axis $P_d = P \cos(\theta)$, where P is the modulus of **P** and θ is the angle between **P** and the ion detection direction. The momentum distribution $\Delta P_d\,(A^{Q+})$ for a particular A^{Q+} ion is related to the time-of-flight distribution $\Delta T\,(A^{Q+})$ following the equation [12]:

$$\Delta P_d(A^{Q+}) \propto Q\,\Delta T(A^{Q+}) \tag{14}$$

Table 3
KER values measured for H^+ ions for the fragmentation channels $H^+ + C^{q+}$ ($q = 1$–3), $H^+ + O^{q+}$ ($q = 1$–2) and $H^+ + H^+$ from Fig. 5

Dissociation products	Ion	KER (eV)	
		E_{prob}	E_{max}
$H^+ + C^+$	H^+	15.5	55.7
$H^+ + C^{2+}$	H^+	37.3	65.0
$H^+ + C^{3+}$	H^+	43.0	64.5
$H^+ + O^+$	H^+	16.8	57.5
$H^+ + O^{2+}$	H^+	37.1	64.8
$H^+ + H^+$	H^+	16.0	84.0

Using the above relationship, we can define a slope between the TOF distributions of correlated ionic species in the coincidence map:

$$\tan\theta = \frac{T_x}{T_y} = \frac{P_x\,Q_y}{P_y\,Q_x} \tag{15}$$

where P and Q are the momentum and charge state of the ions displayed along the x- and y- TOF axis.

The shape of the islands gives information about the fragmentation dynamics of two-body as well as many-body dissociation processes. Figs. 2 and 3 show the coincidence map corresponding to the two-body fragmentation pathway $CH_3OH^{2+} \rightarrow CH_3^+ + OH^+$ (Eq. (1)). Here the ions dissociate in opposite directions with equal momenta $|P_x| = |P_y|$ and the island is aligned along $\theta = -45^\circ$ or -1 slope resulting in a narrow structure perpendicular to the diagonal. For the same reason, we get a slope of -1 for the dissociation pathways assigned by Eqs. (4)–(6), and hydrogen migration channel (Eq. (11)). In case of a many-body fragmentation, the measured slope is influenced by the momenta of the intermediate dissociation products.

Fig. 6 shows the slopes drawn along the coincidence islands represented by Eqs. (4), (8), (9) and (10) respectively from right to left. Here we observe that the dissociation channels depicted by $H^+ + CH_{(3-m)}OH^+$ ($m = 1$–3) obey the slopes drawn along -45° to an exact manner. But the breakup channel $H^+ + CO^+$ deviate to a large extent from -1 slope. Such a possibility had earlier been discussed by Siegmann et al. [13] for the fragmentation patterns of CH_4 in collision with HCI. In collisions with highly charged Ar-ions multiple ionization takes place and undetected charged fragments significantly contribute to the momentum balance. Hence for an event like $H^+ + CO^+$, where further undetected H^+ ions are involved, a smaller amount of momentum will be imparted to the central C–O moiety. Therefore, a slope closer to 'zero' shows that the CO^+ ion nearly stays at rest, whereas the protons emerge with a comparatively large share of momentum.

5. Conclusion

In this article, we have described in detail the different dissociation pathways of multiply charged methanol molecules in collision with HCI. We observed a wide range of dissociation products from the TOF spectrum. From the coincidence map, we had separated out the different breakup phenomena and measured the KER of nearly all breakup pathways. We found that some of them

agree well with values calculated from pure CEM. The geometrical properties of the islands in the coincidence map gives further information about the momentum balance in the fragmentation dynamics of two- or many-body dissociation. Hydrogen migration is observed in case of low energy HCI-induced reactions. It would be interesting to investigate how this rapid migration of hydrogen atoms from one site to another is induced through the coupling with the ion-induced fields.

Acknowledgements

We thankfully acknowledge the staff of Inter-University Accelerator Centre and LEIBF group for providing all necessary facilities. The authors are grateful to D. Kanjilal for effective suggestions throughout the setting up of the apparatus. S.D. thanks the University Grants Commission (UGC) and Inter-University Accelerator Centre (IUAC); J.R., the Council for Scientific and Industrial Research (CSIR), India for providing financial support in the form of fellowship.

References

[1] D. Mathur, Phys. Rep. 391 (2004) 1.
[2] J.H.D. Eland, B.J. Treves-Brown, Int. J. Mass Spectrom. Ion Process. 113 (1992) 167.
[3] E. Ruhl, S.D. Price, S. Leach, J.H.D. Eland, Int. J. Mass Spectrom. Ion Process. 97 (1990) 175.
[4] H. Ren, C. Wu, R. Ma, H. Yang, H. Jiang, Q. Gong, Int. J. Mass Spectrom. 219 (2002) 305.
[5] Y. Furukawa, K. Hoshina, K. Yamanouchi, H. Nakano, Chem. Phys. Lett. 414 (2005) 117.
[6] T. Okino, Y. Furukawa, P. Liu, T. Ichikawa, R. Itakura, K. Hoshina, K. Yamanouchi, H. Nakano, Chem. Phys. Lett. 423 (2006) 220.
[7] S. De, J. Rajput, A. Roy, P.N. Ghosh, C.P. Safvan, Phys. Rev. Lett. 97 (2006) 213201.
[8] S. De, P.N. Ghosh, A. Roy, C.P. Safvan, Nucl. Instr. Methods Phys. Res. B 243 (2006) 435.
[9] S. De, J. Rajput, A. Roy, P.N. Ghosh, C.P. Safvan, J. Chem. Phys. 127 (2007) 051101.
[10] A. Hishikawa, H. Hasegawa, K. Yamanouchi, J. Electron Spectrosc. Relat. Phenomenon 141 (2004) 195200.
[11] J.H.D. Eland, Mol. Phys. 61 (1987) 725.
[12] M.R. Bruce, L. Mi, C.R. Sporleder, R.A. Bonham, J. Phys. B 27 (1994) 5773.
[13] B. Siegmann, U. Werner, R. Mann, Nucl. Instr. Methods Phys. Res. B 233 (2005) 182.